The Journal of Chemical Physics

A practical ansatz for evaluating the electronic friction tensor accurately, efficiently, and in a nearly black-box format

Cite as: J. Chem. Phys. **150**, 164105 (2019); https://doi.org/10.1063/1.5085683
Submitted: 13 December 2018 . Accepted: 20 March 2019 . Published Online: 23 April 2019

Zuxin Jin, and Joseph E. Subotnik

View Online Export Citation CrossMark

ARTICLES YOU MAY BE INTERESTED IN

Perspective: Computational chemistry software and its advancement as illustrated through three grand challenge cases for molecular science
The Journal of Chemical Physics **149**, 180901 (2018); https://doi.org/10.1063/1.5052551

Electronic energy transfer studied by many-body Green's function theory
The Journal of Chemical Physics **150**, 164107 (2019); https://doi.org/10.1063/1.5066290

Perspective: How to understand electronic friction
The Journal of Chemical Physics **148**, 230901 (2018); https://doi.org/10.1063/1.5035412

AIP Publishing

© 2019 Author(s).

The Journal of Chemical Physics ARTICLE scitation.org/journal/jcp

A practical ansatz for evaluating the electronic friction tensor accurately, efficiently, and in a nearly black-box format

Cite as: J. Chem. Phys. 150, 164105 (2019); doi: 10.1063/1.5085683
Submitted: 13 December 2018 • Accepted: 20 March 2019 •
Published Online: 22 April 2019

View Online Export Citation CrossMark

Zuxin Jin and Joseph E. Subotnik

AFFILIATIONS

Department of Chemistry, University of Pennsylvania, Philadelphia, Pennsylvania 19104, USA

ABSTRACT

It is well-known that under conditions of fast electronic equilibration and weak nonadiabaticity, nonadiabatic effects induced by electron-hole pair excitations can be partly incorporated through a frictional force. However, *ab initio* computation of the electronic friction tensor suffers from numerical instability and usually demands a convergence check. In this study, we present an efficient and accurate interpolation method for computing the electronic friction tensor in a nearly black-box manner as appropriate for molecular dynamics. In almost all cases, our method agrees quite well with the exact friction tensor which is available for several quadratic Hamiltonians. As such, we outperform more conventional approaches that are based on the introduction of a broadening parameter. Future work will implement this interpolation approach within *ab initio* software packages.

Published under license by AIP Publishing. https://doi.org/10.1063/1.5085683

I. INTRODUCTION

Nonadiabatic effects are common on metal surfaces because of the ease with which electron-hole pair (EHP) excitations can be created from a continuum of electronic states around the Fermi level whenever there is any non-vanishing nuclear-electronic coupling. Moreover, the creation of EHPs can contribute significantly to molecular dynamical processes on metal surfaces,[1] including adsorption,[2,3] desorption,[4] surface diffusion,[5] and scattering.[6,7] Unfortunately, modeling the exact dynamical role of EHPs on metal surfaces is very challenging,[8] and there are very few methods available today.[9–15] After all, when the electronic state is not the ground state and electronic dynamics are possible, one is necessarily breaking the Born-Oppenheimer (BO) approximation,[16] which is the bedrock of modern quantum chemistry.

Perhaps the most widely used correction to traditional BO dynamics is electronic friction, a correction to ballistic nuclear motion that incorporates some effects of EHP excitations. The molecular dynamics with electronic friction (MDEF) approach[17] evolves nuclei according to a classical Langevin equation

$$M\ddot{R}_\mu = F_\mu - \sum_\nu \gamma_{\mu\nu}\dot{R}_\nu + \zeta_\mu(t), \tag{1}$$

where μ and ν are nuclear coordinate indices, F is the averaged force from adiabatic potential energy surfaces (PES), γ is the electronic friction tensor (EFT), and ζ is the random force.

Equation (1), or $\gamma_{\mu\nu}$ alone, was historically derived via several different approaches.[18] To our knowledge, the first prediction of the EFT for adsorbates on metal surfaces was given by Suhl and co-workers.[19] In their study, the linear response of charge density, current density, and kinetic energy density according to the Fokker-Planck equation was equated to those according to full quantum mechanics using a Kubo formula (a so-called "bootstrap" procedure). Through this comparison, the electronic friction was extracted. An alternative derivation in the framework of Ehrenfest dynamics was given by Head-Gordon and Tully,[17] assuming weak nonadiabaticity. Their resulting EFT was consistent with the vibrational Fermi's golden rule relaxation rate of adsorbates on metal surfaces.[20–23] It is also possible to establish Eq. (1) through path integral approaches[24,25] or through an inspection of the electrochemical electron transfer rate.[26] Recently, another formulation by von Oppen *et al.* was obtained using the non-equilibrium Green's function (NEGF) and scattering matrix approach,[27,28] assuming a mean-field Hamiltonian. More recently, Eq. (1) was derived from the quantum-classical Liouville equation (QCLE) by assuming only

Published under license by AIP Publishing

that electronic states equilibrate much faster than nuclear motion.[29] Finally, through a cumulant expansion performed in the difference between a fully quantum and a classical Hamiltonian, Galperin *et al.* have shown that even if the assumption of slow nuclei is relaxed, one can still find a generalized Langevin equation.[30]

Even though the underlying assumptions of the various approaches above are slightly different, in general, it has been shown that basically all reported EFTs are consistent in the Markovian limit. For instance, the Head-Gordon and Tully friction is consistent with the von Oppen friction,[31] and the von Oppen friction is consistent with the QCLE friction in and out of equilibrium.[32] These findings indicate that there is only one universal electronic friction tensor. Moreover, the assumption of fast electronic equilibration should be valid in many interfacial processes so that there is hope that electronic friction may be able to describe a host of non-BO relaxation processes on metal surfaces, provided that $\Gamma \gg \hbar\omega$, where Γ is the adsorbate-metal hybridization function (i.e., $\hbar/\Gamma$ is the adsorbate electronic lifetime) and ω is a typical molecular frequency.

Now, assuming a quadratic Hamiltonian at equilibrium, the exact EFT takes the following form:[29]

$$\gamma_{\mu\nu} = -\pi\hbar \int_{-\infty}^{+\infty} d\epsilon \mathrm{Tr}(\partial_\mu \mathcal{H}\mathcal{P}(\epsilon)\partial_\nu \mathcal{H}\mathcal{P}(\epsilon)) \frac{\partial f(\epsilon)}{\partial \epsilon}, \quad (2)$$

where $\mathcal{H}$ is the electronic Hamiltonian (that depends parametrically on the nuclear position) and $\mathcal{P}(\epsilon) = \delta(\epsilon - \mathcal{H})$. We reiterate that μ and ν represent nuclear coordinates. Unfortunately, evaluating Eq. (2) represents a big computational challenge. To understand why this is so, note that the integrand in Eq. (2) consists of two parts. On the one hand, $\partial f/\partial\epsilon$ is characterized by k_BT, which is usually a very small energy scale in solid-state systems compared with typical electronic energy scales (bandwidth, hybridization function, etc.). As a reference, k_BT is merely about 26 meV at room temperature. On the other hand, the eigenspectrum of $\mathcal{H}$, denoted $\{\lambda_i\}$, usually covers a very large energy range (e.g., a few electron volts). Thus, without hundreds or thousands of points, there is a mismatch between the relative magnitudes of k_BT and the energy spacings of $\{\lambda_i\}$ around the Fermi level, which can easily lead to numerical error or instability. In particular, it is quite possible that for realistic calculations, the set $\{\lambda_i\}$ will barely sample $\partial f/\partial\epsilon$ even though this set is sufficiently dense to sketch other electronic properties, e.g., the band structure or the spectral function. In general, calculating the electronic friction has proven to be very difficult and finicky, especially if one wants to minimize the number of k points in the Brillouin zone sampling.

From the form of Eq. (2), one may recognize the similarity between the electronic friction and the electron-phonon (el-ph) coupling strength

$$\lambda_{\boldsymbol{q}\nu} = \frac{1}{\rho(\epsilon_F)\omega_{\boldsymbol{q}\nu}} \sum_{mn} \int_{\mathrm{B.Z.}} \frac{d\boldsymbol{k}}{\Omega_{\mathrm{B.Z.}}} |g_{mn,\nu}(\boldsymbol{k},\boldsymbol{q})|^2 \delta(\epsilon_{n\boldsymbol{k}} - \epsilon_F)\delta(\epsilon_{m\boldsymbol{k}+\boldsymbol{q}} - \epsilon_F) \quad (3)$$

at $\boldsymbol{q} = 0$, where $\rho(\epsilon_F)$ is the density of states (DOS) at the Fermi level, $\omega_{\boldsymbol{q}\nu}$ is the frequency of phonon of wavevector $\boldsymbol{q}$ and branch index ν, and

$$g_{mn,\nu}(\boldsymbol{k},\boldsymbol{q}) = \frac{1}{\sqrt{2\omega_{\boldsymbol{q}\nu}}} \langle \psi_{m\boldsymbol{k}+\boldsymbol{q}} | \partial_{\boldsymbol{q}\nu} V | \psi_{n\boldsymbol{k}} \rangle. \quad (4)$$

Here, $\partial_{\boldsymbol{q}\nu}V$ is the derivative of the self-consistent potential associated with the phonon indexed by $\boldsymbol{q}\nu$, and $\psi_{n\boldsymbol{k}}$ is the electronic wavefunction for band n and wavevector $\boldsymbol{k}$. To compute the electronic friction, one could follow well-established el-ph methods, e.g., a Wannier interpolation followed by a Gaussian smearing.[33–35] Alternatively, one could apply a periodic self-consistent calculation over a big unit cell and a Gaussian smearing afterward. We should note that for these smearing-based methods, an additional parameter (here denoted σ) emerges, characterizing the width of the broadening/smearing functions. This additional parameter σ has no intrinsic physical meaning but is only a numerical artifact that is necessary in order to integrate over an infinite bath using a finite set of states. In practice, results computed in this manner are considered acceptable as long as they do not significantly depend on the broadening parameter σ (within a certain range, of course). In an ideal world, σ will be arbitrarily small as we would work with a sufficiently dense set of bath states (corresponding to a massive, effectively infinite solid). However, in realistic simulations, one can only afford a finite number of bath states and the convergence with respect to σ is not always guaranteed.[36] As such, a convergence study is usually required, which prevents the algorithm from being a black-box tool for an MDEF simulation. Moreover, a periodic calculation with a large unit cell can be expensive. Altogether, these disadvantages suggest that broadening schemes may not be optimal for computing EFTs in the context of on-the-fly simulations. Besides these broadening-based methods, the other standard solid-state approach for computing the EFTs is the tetrahedron method,[36,37] whereby one slowly isolates the shape of the Fermi surface in reciprocal space. This method is optimal at zero temperature, but it is not obvious how to extend the method for large non-periodic systems. Finally, we emphasize that, thus far, no one has checked whether or not these standard el-ph methods predict the correct EFT for the quadratic Hamiltonian—where one can derive analytical expressions for the EFT.

The only other alternative nowadays to standard el-ph methods is the local density friction approximation (LDFA).[10,12,21,38–41] According to the LDFA, the electronic friction is computed by assuming that atoms move in a homogeneous free electron gas with the electronic charge density set equal to the metallic charge density where the atoms are placed. As such, $\gamma_{\mu\nu}$ is isotropic by construction. However, in recent studies,[13,15,42] *ab initio* calculations show that $\gamma_{\mu\nu}$ can be anisotropic and sometimes significantly non-diagonal in either normal modes or crystallographic coordinates. This finding indicates that EHP-induced nonadiabatic couplings can lead to friction-induced intra-molecular energy redistribution and a complete electronic friction tensor will be necessary to study the accurate dynamical processes. For our purposes, the LDFA cannot be applied to model Hamiltonians, hence will not be benchmarked below.

Overall, the motivation of this study is to establish a fast, (nearly) black-box algorithm for computing the electronic friction. The paper is organized as follows. In Sec. II, we review several different methods for calculating electronic friction tensors in a quadratic Hamiltonian. These methods include (i) Gaussian broadening (GB), (ii) off diagonal normalized Gaussian broadening (ONGB), and (iii) direct quadrature (DQ). Also, we present the exact solution for the EFT when possible. Finally, with insight from the exact solution, we introduce our new scheme, an interpolation of the cumulative sum

Published under license by AIP Publishing

of orbital energy gradients (ICSOEG). In Sec. III, we benchmark most of the methods above against three different model Hamiltonians. In Sec. IV, we discuss the advantages and usefulness of our interpolation method and the future possibility for an *ab initio* implementation. We conclude in Sec. V.

II. METHODS

We will now review several existing methods for evaluating Eq. (2), and we will also introduce a new approach. Before doing so, however, we note that electronic friction tensors can be exactly evaluated in certain cases. Consider a system-bath-coupling model described by the following quadratic Hamiltonian:

$$\mathcal{H} = h(\boldsymbol{R})d^\dagger d + \sum_l \epsilon_l c_l^\dagger c_l + \left(\sum_l V_l(\boldsymbol{R}) c_l^\dagger d + \text{h.c.}\right). \tag{5}$$

Here, $d(d^\dagger)$ is the operator corresponding to an impurity state and $c_l(c_l^\dagger)$ is the operator corresponding to the bath state l whose energy is ϵ_l. Both the impurity on-site energy h and system-bath coupling V have a dependence on a parameter $\boldsymbol{R}$, which may represent any nuclear coordinate(s). The bath states are assumed to be sufficiently dense to form a quasi-continuum.

In the wideband limit, the exact analytical expression, as found with a nonequilibrium Green's function (NEGF) approach, is[24,27,28,43]

$$\gamma_{\mu\nu}^{WB} = -\pi\hbar \int \mathrm{d}\epsilon \left(\partial_\mu h + (\epsilon - h)\frac{\partial_\mu \Gamma}{\Gamma}\right)\left(\partial_\nu h + (\epsilon - h)\frac{\partial_\nu \Gamma}{\Gamma}\right) A^2(\epsilon)\frac{\partial f}{\partial \epsilon}. \tag{6}$$

Here, $\Gamma = 2\pi \sum_l V_l^2 \delta(\epsilon - \epsilon_l)$ is the hybridization function (which is a constant of ϵ in the wideband limit), and

$$A(\epsilon) = \frac{1}{\pi}\frac{\Gamma/2}{(\epsilon - h)^2 + (\Gamma/2)^2} \tag{7}$$

is the spectral function. If we go beyond the wideband limit, the relevant terms in Eq. (6) should be replaced by the following:[44]

$$h \to \tilde{h}(\epsilon) = h + \mathrm{Re}(\Sigma(\epsilon)) = h + \text{p.p.} \sum_l \frac{|V_l|^2}{\epsilon - \epsilon_l}, \tag{8}$$

$$\Gamma \to \Gamma(\epsilon) = 2\pi \sum_l |V_l|^2 \delta(\epsilon - \epsilon_l) \approx 2\pi |V(\epsilon)|^2 \rho(\epsilon), \tag{9}$$

$$A(\epsilon) \to \tilde{A}(\epsilon) = \frac{1}{\pi}\frac{\Gamma(\epsilon)/2}{(\epsilon - \tilde{h}(\epsilon))^2 + (\Gamma(\epsilon)/2)^2}. \tag{10}$$

Here p.p. stands for the principal part. For details, see Eq. (17) in Ref. 45 and Eq. (52) in Ref. 31.

As a practical matter, it is important to note that while evaluating Eq. (6) is straightforward for certain toy model problems where the density of states $\rho(\epsilon)$ and hybridization $\Gamma(\epsilon)$ are smoothly dependent on energy ϵ, it can be tricky to evaluate Eqs. (6)–(10) for other models where $\rho(\epsilon)$ and $\Gamma(\epsilon)$ may not be very smooth. For example, in *ab initio* Green's function calculations, a contour deformation technique is usually invoked for numerical stability.[46,47] As a general rule, evaluating the spectrum function and the hybridization function is numerically challenging. As such, we expect that Eq. (6) would be nontrivial to implement for an *ab initio* mean field calculation.

For this reason, we will now focus on other methods that are feasible for evaluating the electronic friction tensor in Eq. (2) in general. Our list, though not comprehensive, should give the correct overall state of affairs.

A. Gaussian broadening (GB)

In a single-orbital basis, Eq. (2) can be reduced to

$$\gamma_{\mu\nu}^{GB} = -\pi\hbar \sum_{ij} (\partial_\mu \mathcal{H})_{ij} (\partial_\nu \mathcal{H})_{ji} \delta(\lambda_i - \lambda_j) \left.\frac{\partial f}{\partial \epsilon}\right|_{\lambda_i}, \tag{11}$$

where $i(j)$ refers to a Kohn-Sham orbital with energy $\lambda_i(\lambda_j)$. The Dirac deltas are usually replaced by a peak-shaped function $\hat{\delta}(\lambda_i - \lambda_j; \sigma)$ in practical implementations, where σ is the broadening parameter. A common choice is Gaussian smearing

$$\hat{\delta}(\lambda_i - \lambda_j; \sigma) = \frac{1}{\sigma\sqrt{2\pi}} \mathrm{e}^{-\frac{(\lambda_i - \lambda_j)^2}{2\sigma^2}}. \tag{12}$$

The advantage of Eq. (11) is the ease of evaluation. The disadvantage of Eq. (11) is that, as mentioned before, verifying the convergence with respect to σ can be time-consuming. Moreover, the existence of such convergence may not be guaranteed without a sufficiently dense set $\{\lambda_i\}$.

B. Off diagonal normalized Gaussian broadening (ONGB)

The friction tensor can also be extracted by a careful consideration of a vibrational relaxation process. In particular, one may attribute vibrational relaxation to a frictional effect and extract the friction tensor from the Fermi's golden rule rate, which yields[22,23,42]

$$\gamma_{\mu\nu}^{ONGB} = \pi\hbar \sum_i \sum_{j\neq i} (\partial_\mu \mathcal{H})_{ij} (\partial_\nu \mathcal{H})_{ji} \delta(\lambda_i - \lambda_j) \frac{f(\lambda_i) - f(\lambda_j)}{\lambda_i - \lambda_j}. \tag{13}$$

Interestingly, Eq. (13) contains only the off diagonal elements of $\partial_\mu \mathcal{H}$. Every single term in Eq. (13) is effectively the product of two derivative couplings multiplied by an electronic DOS. This relationship stands in contrast to Eq. (11), which is dominated by the diagonal terms. Nonetheless, one might expect that Eq. (13) should recover Eq. (11) in the continuum limit since $\delta(\lambda_i - \lambda_j)$ suggests that only states with nearly degenerate energies can contribute, in which case $(f(\lambda_i) - f(\lambda_j))/(\lambda_i - \lambda_j)$ approaches $\partial f/\partial \epsilon|_{\lambda_i}$.

Similar to the method in Sec. II A, for implementation purposes, the Dirac delta functions have to be replaced by some broadening functions. In a recent study,[42] the broadening function was proposed to be

$$\tilde{\delta}(\lambda_i - \lambda_j; \sigma) = \frac{\hat{\delta}(\lambda_i - \lambda_j; \sigma)}{1 - \mathrm{erf}(\lambda_i - \lambda_j)}, \tag{14}$$

where $\hat{\delta}(\lambda_i - \lambda_j; \sigma)$ is the previous Gaussian broadening function [Eq. (12)]. Once $(\partial_\mu \mathcal{H})_{ij}$ and $\{\lambda_i\}$ are obtained, evaluating Eq. (13)

Published under license by AIP Publishing

becomes straightforward. However, as we will show below, γ^{ONGB} faces similar convergence problems as does γ^{GB}.

C. Direct quadrature (DQ) with density of states

Yet another way to evaluate the electronic friction tensor and tame the Dirac delta functions in Eq. (2) is to note that (assuming no degeneracy)

$$\delta(\lambda_i - \lambda_j) = \sum_l \delta(\lambda_i - \lambda_l)\delta_{jl} = \sum_l \delta(\lambda_i - \lambda_l)\delta_{ji} = \rho(\lambda_i)\delta_{ji}, \quad (15)$$

which yields

$$\gamma_{\mu\nu}^{DQ} = \pi\hbar \sum_i (\partial_\mu \mathcal{H})_{ii}(\partial_\nu \mathcal{H})_{ii}\rho(\lambda_i) \left.\frac{\partial f}{\partial \epsilon}\right|_{\lambda_i}. \quad (16)$$

Here, we have used the shorthand DQ to stand for direct quadrature.

One might correctly fear that Eq. (16) would be unreliable unless the eigenspectrum $\{\lambda_i\}$ was sufficiently dense to sample $\partial f/\partial\epsilon$, which is usually not possible in practice. And there is a natural challenge in Eq. (16): how to calculate the DOS $\rho(\lambda_i)$? Even so, Eq. (16) can give us some qualitatively correct information about electronic friction tensors, and we will present several results later.

D. Interpolation of the cumulative sum of orbital energy gradients (ICSOEG)

We will now present a fourth and final algorithm for evaluating the electronic friction tensors, which we believe finds the optimal balance between accuracy and stability.

As mentioned earlier, the integrand in Eq. (2) is the product of two functions with very different energy scales: $\partial f/\partial\epsilon$ is characterized by k_BT, while $\mathrm{Tr}(\partial_\mu \mathcal{HP}(\epsilon)\partial_\nu \mathcal{HP}(\epsilon))$ is characterized by a typical electronic energy; the latter is usually much larger than the former. With such a separation of energy scales, obviously, one can approximate the slowly varying function to be of a relatively simple form locally. Therefore, an interpolation method would appear to be well justified. Thus, our goal henceforth will be to approximate $\mathrm{Tr}(\partial_\mu \mathcal{HP}(\epsilon)\partial_\nu \mathcal{HP}(\epsilon))$ by a simple function in the region where $\partial f/\partial\epsilon$ is significant.

For such an interpolation scheme, we require (i) $\mathrm{Tr}(\partial_\mu \mathcal{HP}(\epsilon)\partial_\nu \mathcal{HP}(\epsilon))$ evaluated at energy eigenvalues $\{\lambda_i\}$ and (ii) an appropriate functional form. We begin with item (i). According to Eq. (15), if there is no degeneracy, we can focus on the expression

$$\mathrm{Tr}(\partial_\mu \mathcal{HP}(\lambda_i)\partial_\nu \mathcal{HP}(\lambda_i)) = (\partial_\mu \mathcal{H})_{ii}\rho(\lambda_i)(\partial_\nu \mathcal{H})_{ii}\rho(\lambda_i). \quad (17)$$

Notice that the pair of problematic Dirac delta functions has not been removed; instead, one problem has been transformed into another: now, we must evaluate the DOS ($\rho(\lambda_i)$). Next, if we turn to Eq. (15) again, it is simple to show that

$$(\partial_\mu \mathcal{H})_{ii}\rho(\lambda_i) = \mathrm{Tr}(\partial_\mu \mathcal{HP}(\lambda_i)). \quad (18)$$

Therefore, instead of fitting the function $\Omega_{\mu\nu}(\epsilon) \equiv \mathrm{Tr}(\partial_\mu \mathcal{HP}(\epsilon)\partial_\nu \mathcal{HP}(\epsilon))$, it is actually sufficient to fit the function $Z_\mu(\epsilon) \equiv \mathrm{Tr}(\partial_\mu \mathcal{HP}(\epsilon))$. Obviously, $\Omega_{\mu\nu}(\epsilon)$ is a quadratic function of $Z_\mu(\epsilon)$; such a splitting of the electronic friction tensor might be expected from the factorization in Eq. (6). Finally, we still need to deal with the DOS (i.e., delta functions) in $Z_\mu(\epsilon)$. To that end, we will define

$$I_\mu(\lambda_i) \equiv \int_{-\infty}^{\lambda_i} d\epsilon \mathrm{Tr}(\partial_\mu \mathcal{HP}(\epsilon)) \approx \sum_{j=0}^{i} \langle j|\partial_\mu \mathcal{H}|j\rangle. \quad (19)$$

By fitting $I_\mu(\epsilon)$ instead of $Z_\mu(\epsilon)$, the singularity of delta functions has been completely removed.

At this point, let us turn to item (ii). The functional form to fit $I(\epsilon)$ must be carefully selected. At sufficiently low temperatures, it suffices to fit $I(\epsilon)$ as a polynomial

$$\tilde{I}_\mu^{poly}(\epsilon) = \sum_{p=0}^{N} a_{\mu,p}(\epsilon - \epsilon_F)^p, \quad (20)$$

where ϵ_F is the Fermi level and N is the order of the polynomial. As such,

$$\gamma_{\mu\nu} \approx -\pi\hbar \int_{-\infty}^{+\infty} d\epsilon \frac{d\tilde{I}_\mu^{poly}}{d\epsilon}\frac{d\tilde{I}_\nu^{poly}}{d\epsilon}\frac{\partial f}{\partial\epsilon} \quad (21)$$

$$= \pi\hbar\left[a_{\mu,1}a_{\nu,1} + \frac{\pi^2}{3}\left(4a_{\mu,2}a_{\nu,2} + 3a_{\mu,1}a_{\nu,3} + 3a_{\nu,1}a_{\mu,3}\right)(k_BT)^2 + \ldots\right]. \quad (22)$$

However, for reasonably large temperatures, the polynomial ansatz in Eq. (20) will not be optimal to sketch $I_\mu(\epsilon)$. To that end, we would like to find another functional form.

Fortunately, the wideband model discussed in Eqs. (5) and (6) provides us with such an expression. Note that Eq. (6) can be readily rewritten to give $\tilde{I}(\epsilon)$ of the form

$$\tilde{I}_\mu^{WB}(\epsilon) = \frac{1}{\pi}\int^{\epsilon} d\epsilon' \left(\frac{\Gamma/2}{(\epsilon' - h)^2 + (\Gamma/2)^2}\partial_\mu h + \frac{(\epsilon' - h)/2}{(\epsilon' - h)^2 + (\Gamma/2)^2}\partial_\mu \Gamma\right). \quad (23)$$

In other words, $\tilde{I}(\epsilon)$ is the integral of a Lorentzian and antisymmetric Lorentzian. Based on the fact that many real systems can be modeled in the wideband approximation, it would make sense to use the functional form in Eq. (23) as an ansatz. The integration can be performed analytically so that we must fit $I_\mu(\epsilon)$ to the following functional form:

$$\tilde{I}_\mu(\epsilon) = a_0 + a_1 \arctan\left(\frac{\epsilon - a_3}{a_4}\right) + a_2 \ln\left[1 + \left(\frac{\epsilon - a_3}{a_4}\right)^2\right]. \quad (24)$$

Let us now summarize our interpolation algorithm (ICSOEG) step by step for computing the EFT.

i. Find the eigenenergies $\{\lambda_j\}$ and orbital response $\langle j|\partial_\mu \mathcal{H}|j\rangle$;
ii. Align $\langle j|\partial_\mu \mathcal{H}|j\rangle$ according to the ascending order of $\{\lambda_j\}$ and calculate the cumulative sum $I_\mu(\lambda_i) = \sum_{j<i}\langle j|\partial_\mu \mathcal{H}|j\rangle$;
iii. Fit $(\lambda_i, I_\mu(\lambda_i))$ to a smooth function $\tilde{I}_\mu(\epsilon)$ in the vicinity of the Fermi level. In practice, we recommend two curve fits: one using the ansatz deduced from the wideband analysis

Published under license by AIP Publishing

[Eq. (24)] and the other using a polynomial fit [Eq. (20)]. The fit with the smaller residual should be accepted;

iv. Numerically evaluate the friction on a tight grid

$$\gamma_{\mu\nu}^{ICSOEG} = -\pi\hbar \int_{\epsilon_F - W}^{\epsilon_F + W} \mathrm{d}\epsilon \frac{\mathrm{d}\tilde{I}_\mu}{\mathrm{d}\epsilon} \frac{\mathrm{d}\tilde{I}_\nu}{\mathrm{d}\epsilon} \frac{\partial f}{\partial \epsilon}, \tag{25}$$

where W can be a few $k_B T$.

E. Caveats

In a moment, we will present results comparing EFTs as calculated by all methods above (plus the exact answer). Before presenting such results, however, a few caveats need to be addressed.

1. Is electronic friction valid?

It is very important to note that one cannot determine whether or not MDEF is valid by computing $\gamma_{\mu\nu}$ alone. Obviously, one can calculate Eq. (2) or (6) for large or small Γ. However, as mentioned earlier, Eq. (1) is itself valid only under the assumption of weak-nonadiabaticity or fast electronic equilibration (or similar assumptions), which should imply γ is small. Thus, one can always question the meaning of the EFTs that are evaluated by the above methods, especially when Γ is relatively small at a diabatic crossing (so that γ is big). To be more precise, assuming that one can estimate Γ during the curve fitting procedures [note that the parameter a_4 in Eq. (24) should be exactly Γ/2 in the wideband limit] as well as a molecular frequency ω (or some other characteristic time scale related to the molecular dynamics), $\hbar\omega/\Gamma$ can be used as a dimensionless, hopefully small perturbative parameter indicating the validity of MDEF. Beyond this rule of thumb, delineating exactly when MDEF is valid remains an active question of research,[14,48,49] which is beyond the scope of the present paper.

2. How many eigenstates are required?

In a typical solid-state calculation containing an adsorbate and a metal slab, the bath spectrum is determined by the size of the metal slab and the Brillouin zone sampling. In practice, for efficiency, one always prefers a smaller unit cell and fewer Brillouin zone k points, as long as the result is converged. An inevitable question is then, how many bath states do we need to obtain a converged electronic friction. From the analysis of the wideband model, we know that at minimum, the energy spacing between bath states should be much less than Γ, i.e., $\Delta\lambda \ll \Gamma$, so that bath states can sketch out the spectral function. We expect that this necessary condition is also sufficient for calculating an EFT and preliminary evidence below would appear to confirm our intuition, at least for some models that go beyond the wideband limit.

3. Degeneracy

The key steps in establishing the interpolation method, Eqs. (17) and (18), are based on Eq. (15), which holds true only when the electronic Hamiltonian is not degenerate. In reality, of course, no such assumption can always be true, especially given Kramers degeneracy (assuming time-reversal symmetry). Moreover, for materials extended in two or three dimensions, a degenerate subspace is guaranteed and forms a one or two-dimensional manifold. As a result, Eqs. (17) and (18) cannot be universally correct.

Nevertheless, that being said, for periodic calculations, the interpolation method in Sec. II D should remain valid in most situations. Since $\partial_\mu \mathcal{H}$ (in the limit of $q = 0$, where q is the phonon wavevector) and $\mathcal{P}$ are both block-diagonal in crystal momentum k, Eq. (2) is essentially a Brillouin zone summation[50]

$$\gamma_{\mu\nu}^{k-ind.} = -\pi\hbar \int_{-\infty}^{+\infty} \mathrm{d}\epsilon \left(\frac{1}{N_k} \sum_k \mathrm{Tr}\left(\partial_\mu \mathcal{H}^{(k)} \mathcal{P}^{(k)}(\epsilon) \partial_\nu \mathcal{H}^{(k)} \mathcal{P}^{(k)}(\epsilon) \right) \right) \times \frac{\partial f(\epsilon)}{\partial \epsilon} = \frac{1}{N_k} \sum_k \gamma_{\mu\nu}^{(k)}. \tag{26}$$

Suppose we now perform an interpolation method for each independent $\gamma_{\mu\nu}^{(k)}$ with the cumulative sum

$$I_\mu^{(k)}(\lambda_{ik}) = \sum_{j<i} \langle jk | \partial_\mu \mathcal{H}^{(k)} | jk \rangle. \tag{27}$$

When the electronic friction tensor is computed according to Eqs. (26) and (27), let us denote the final answer $\gamma_{\mu\nu}^{k-\mathrm{ind.}}$, which is an average over $\gamma_{\mu\nu}^{(k)}$. For a general interfacial system, degeneracy at a single k point will be uncommon, and so our interpolation method should be safely applicable if we work always separately with each k block.

Finally, although Eqs. (26) and (27) should be valid most often, these equations may not necessarily provide a practical solution. Within each k block, the number of $(\lambda_{ik}, I_\mu^{(k)}(\lambda_{ik}))$ points used for curve fitting is the number of bands. Without a large unit cell, it is unlikely to sufficiently sample the vicinity of the Fermi level. That being said, curve fitting would not be stable.

One tempting approximation is to give up the band picture at the risk of introducing the degeneracy problem. As such, one can compute the "k-gathered" cumulative sum

$$I_\mu(\lambda_{ik}) = \frac{1}{N_k} \sum_{jk'}^{\lambda_{jk'} < \lambda_{ik}} \langle jk' | \partial_\mu \mathcal{H}^{(k')} | jk' \rangle, \tag{28}$$

which will be much denser than $I_\mu^{(k)}$. After calculating $\tilde{I}_\mu$ and $\tilde{I}_\nu$ by the curve fitting procedure in Sec. II D, the friction tensor can then be directly computed by Eq. (25) rather than by averaging over independent k components. To quantify this approximation, let

$$D_\mu^k(\lambda) \equiv \frac{1}{\Delta\lambda} \sum_i^{\lambda < \lambda_{ik} < \lambda + \Delta\lambda} \langle ik | \partial_\mu \mathcal{H}^{(k)} | ik \rangle \tag{29}$$

be the energy-averaged sum of the orbital energy gradients whose orbital energies lie within $(\lambda, \lambda + \Delta\lambda)$ with wavevector k. Furthermore, let

$$\Delta_\mu^k(\lambda) \equiv D_\mu^k(\lambda) - \frac{1}{N_k} \left(\sum_k D_\mu^k(\lambda) \right). \tag{30}$$

Now,

$$\gamma_{\mu\nu}^{k-ind.} = -\pi\hbar \int_{-\infty}^{+\infty} \mathrm{d}\epsilon \left(\frac{1}{N_k} \sum_k \frac{\mathrm{d}\tilde{I}_\mu^{(k)}}{\mathrm{d}\epsilon} \frac{\mathrm{d}\tilde{I}_\nu^{(k)}}{\mathrm{d}\epsilon} \right) \frac{\partial f}{\partial \epsilon}, \tag{31}$$

Published under license by AIP Publishing

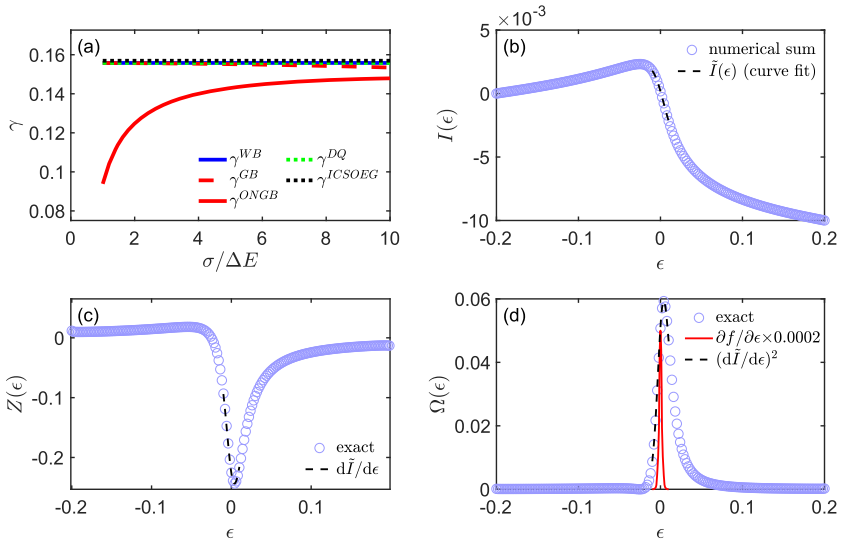

FIG. 1. A wideband model for the Hamiltonian in Eq. (5); $kT = 0.001$, the friction is evaluated at the diabatic crossing point x_0, i.e., $h(x_0) = 0$. The remaining parameters are chosen that $\partial_x h = -0.01$, $\Gamma = 0.028$, $\partial_x\Gamma = -0.011$, and $\epsilon_F = 0$. The bath energy spacing is $\Delta E = 0.0002$ so that $\Gamma/\Delta E = 140$, $k_BT/\Delta E = 5$. (a) Friction tensors computed by Gaussian broadening (γ^{GB}) and off diagonal normalized Gaussian broadening (γ^{ONGB}) vs the broadening parameter σ [see Eqs. (12) and (14)]. The friction tensors computed by direct quadrature (γ^{DQ}), our interpolation method (γ^{ICSOEG}), and the exact wideband solution (γ^{WB}) are also plotted for reference. (b) $I(\epsilon) \equiv \int^{\epsilon} \mathrm{d}\epsilon' \mathrm{Tr}(\partial_x \mathcal{H}\mathcal{P}(\epsilon'))$ vs ϵ. Here, we plot the cumulative sum expression for $I(\epsilon)$ [Eq. (19)] and the fitted curve in the ICSOEG procedure ($\tilde{I}(\epsilon)$). (c) $Z(\epsilon) \equiv \mathrm{Tr}(\partial_x \mathcal{H}\mathcal{P}(\epsilon))$ as a function of ϵ. $Z(\epsilon)$ is evaluated at the eigenenergies of $\mathcal{H}$ according to Eq. (18). The asymmetric shape comes from non-Condon effects ($\partial_x\Gamma \neq 0$). (d) $\Omega(\epsilon) \equiv \mathrm{Tr}(\partial_x \mathcal{H}\mathcal{P}(\epsilon)\partial_x \mathcal{H}\mathcal{P}(\epsilon)) \approx (Z(\epsilon))^2$ as a function of ϵ. $\partial f/\partial\epsilon$ is also plotted for reference. In (b)–(d), for the sake of visual clarity, we plot the exact expressions (blue circles) only every tenth eigenenergies. The ONGB result has the largest error (about 5%). For the most part, all of the methods agree well with the exact wideband expression.

$$\gamma_{\mu\nu}^{k-gathered} = -\pi\hbar \int_{-\infty}^{+\infty} \mathrm{d}\epsilon \left(\frac{\mathrm{d}\tilde{I}_\mu}{\mathrm{d}\epsilon} \frac{\mathrm{d}\tilde{I}_\nu}{\mathrm{d}\epsilon} \right) \frac{\partial f}{\partial \epsilon}, \tag{32}$$

where $\tilde{I}$'s in Eqs. (31) and (32) are the fitted curves of Eqs. (27) and (28), respectively. The difference between $\gamma_{\mu\nu}^{k-ind.}$ and $\gamma_{\mu\nu}^{k-gathered}$ can be seen from the difference between the two terms in the brackets

$$\begin{aligned} &\frac{1}{N_k}\sum_k \frac{\mathrm{d}I_\mu^{(k)}}{\mathrm{d}\epsilon}\frac{\mathrm{d}I_\nu^{(k)}}{\mathrm{d}\epsilon}\bigg|_\lambda - \frac{\mathrm{d}I_\mu}{\mathrm{d}\epsilon}\frac{\mathrm{d}I_\nu}{\mathrm{d}\epsilon}\bigg|_\lambda \\ &= \frac{1}{N_k}\sum_k \left(D_\mu^k(\lambda) D_\nu^k(\lambda) \right) - \frac{1}{N_k^2}\left(\sum_k D_\mu^k(\lambda) \right)\left(\sum_k D_\nu^k(\lambda) \right) \\ &= \frac{1}{N_k}\sum_k \left(\Delta_\mu^k(\lambda)\Delta_\nu^k(\lambda) \right). \end{aligned} \tag{33}$$

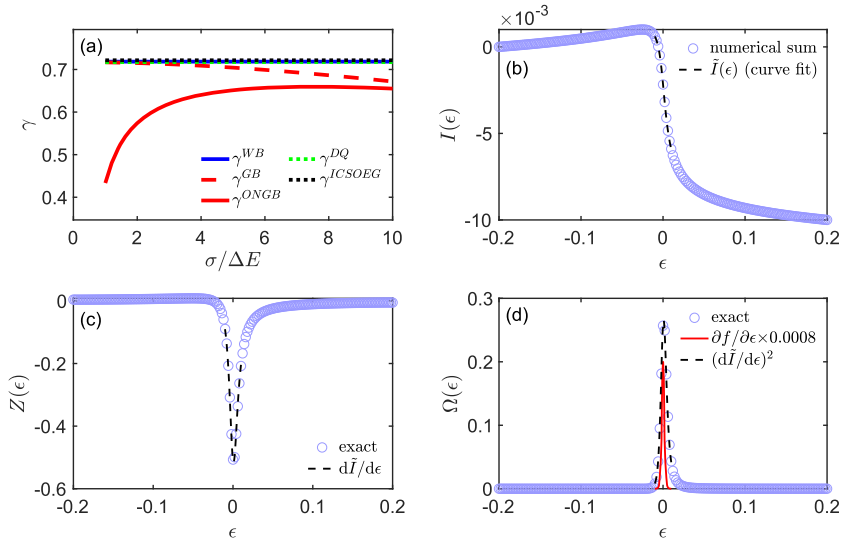

FIG. 2. (a)-(d) Same as in Fig. 1 with the only change of parameters being that we now set $\Gamma = 0.013$ and $\partial_x\Gamma = -0.005$. For this choice of parameters, we have chosen Γ to be smaller so that there are fewer eigenstates spread out over the spectrum of interest. In (a), notice that even though $\Gamma/\Delta E = 65$ is still quite large and $k_BT/\Delta E = 5$ remains unaltered, results from the broadening methods (γ^{GB} and γ^{ONGB}) deteriorate. By contrast, our interpolation method remains stable.

Published under license by AIP Publishing

In other words, the "k-gathered" approach essentially neglects the fluctuations of orbital energy gradients within the degenerate subspace. As shown below, this approximation can be quite good.

III. RESULTS

In this section, we will compare our interpolation scheme with all of the other three methods in Secs. II A–II C when possible. We focus on three different model problems: (1) a flat-band model, (2) a quasi-continuous system-bath-coupling model, and (3) a periodic tight binding model containing a molecular site and a slab. The last two models go beyond the wideband approximation, and all of the three models go beyond the Condon limit.

A. Flatband model

Consider a model described by the Hamiltonian in Eq. (5). Assume that the bath levels (ϵ_l) are evenly spaced and sufficiently wide and that all system-bath couplings (V_l) are identical. For simplicity, we assume that the parameter $\boldsymbol{R}$ has only one degree of freedom, denoted by x. In Figs. 1–4, we benchmark the electronic friction tensors according to all the methods in Sec. II for a variety of bath DOS, temperatures, and hybridization functions (Γ).

As illustrated in Fig. 1, with the assumptions above, given a sufficiently dense bath and large Γ (so that the model is in the wideband limit), basically all of the methods in Sec. II agree very well with the exact solution given by the NEGF expression [Eq. (6)]. Among these approaches, the largest error happens to be the off diagonal normalized Gaussian broadening method, which is about 5%; even so, the error is small.

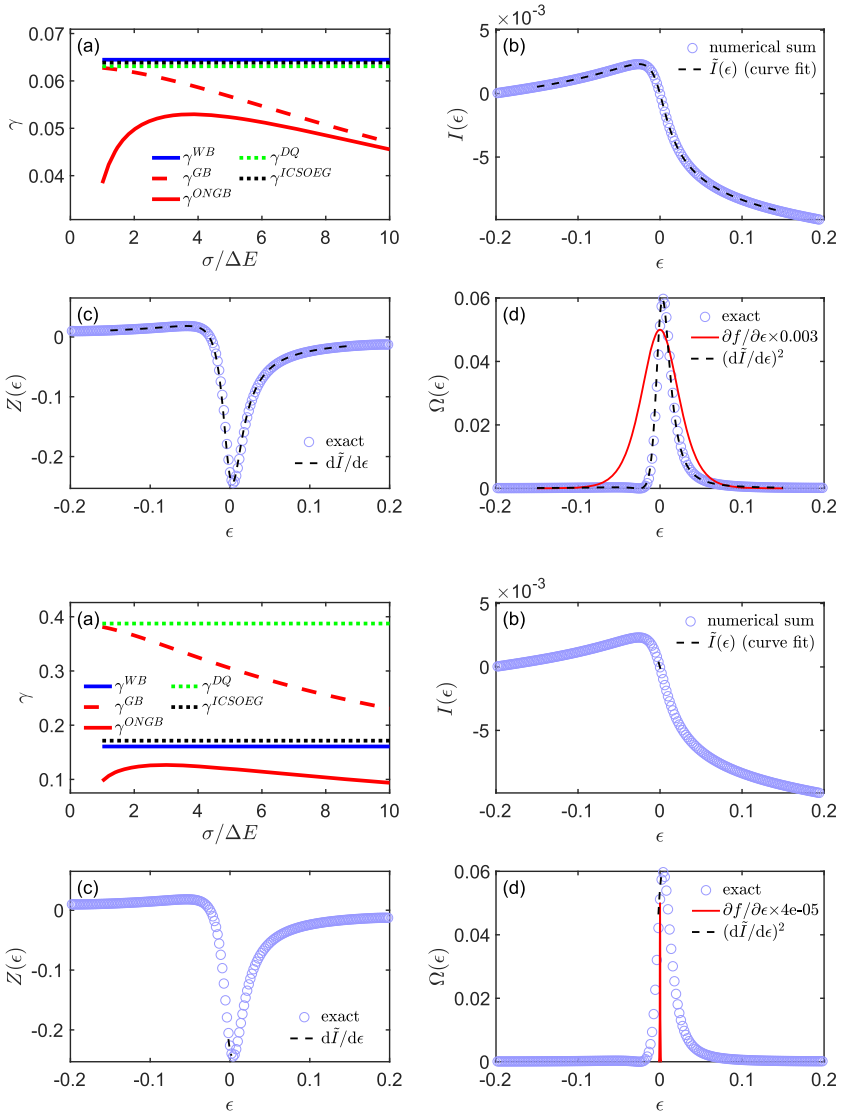

FIG. 3. (a)-(d) Same as in Fig. 1 except that now kT = 0.015 and the bath contains only 200 states (ΔE = 0.002). Here, the temperature is comparable to Γ ($\Gamma/\Delta E$ = 14, $k_BT/\Delta E$ = 7.5). However, observe that in (a), the broadening methods fail to converge with respect to the broadening parameter due to a poor quasi-continuity. These results highlight that broadening methods can fail even in the high-T limit if there is not enough sampling. By contrast, our interpolation method still agrees very well with the exact wideband result.

FIG. 4. (a)-(d) Same as in Fig. 3 except that kT = 0.0002. Now, $\Gamma/\Delta E$ = 14 and $k_BT/\Delta E$ = 0.1. This low-T case represents the most difficult situation for broadening methods: both Γ and k_BT are very small. As shown in (a), our interpolation method remains relatively stable, while other methods either do not yield a correct result or even fail to converge with respect to the broadening parameter.

Published under license by AIP Publishing

In Figs. 2–4, we present γ in different situations that deviate from the ideal wideband limit to the extent that we undersample the bath states such that the spectral function of the impurity is sampled by fewer energy eigenvalues. Fig. 2 shows that even with a flatband of seemingly dense bath states, results from the broadening methods can be less robust. A more significant example is shown in Fig. 3, in which the bath has a DOS that is 1/10 of the previous one and can no longer serve as a quasi-continuum. Results from the two broadening methods fail to converge in this case, even though the temperature is relatively high ($k_BT/\Gamma \approx 0.53$). At the same time our interpolation remains stable, which is perhaps not surprising since the functional form used in curve fitting is selected based on a wideband model. Figure 4 shows that results from the broadening methods and direct quadrature can further deteriorate if the system is equilibrated at a low temperature. A similar situation naturally occurs for realistic solid-state electron-phonon calculations, where the Brillouin zone sampling is usually very sparse in a self-consistent field calculation as compared with k_BT. In practice, a Wannier (Fourier) interpolation is often invoked to generate a dense $k-$grid before Gaussian broadening so as to recover the necessary quasi-continuum.[35] Such an approach is very useful in Brillouin-zone integrations (having been applied in many calculations) and may be worth exploring in the future.

For our purposes, we report that our interpolation method always remains relatively stable. Note that although the curve fitting is still accurate, the relative difference between γ^{ICSOEG} and γ^{NEGF} increases to about 7%. We believe this error is systematic and originates because the condition of the bath being a quasi-continuum, upon which Eq. (6) is based, is less robust in Fig. 4.

B. Quasi-continuous model

In Sec. III A, we studied a model that mimicked the wideband limit, which is usually only a rough approximation of a true solid state system. Now, we will investigate how the methods in Sec. II behave when systems go beyond that limit. Here, exact solutions are still available through Eq. (6) with the modifications listed in Eqs. (8)–(10).

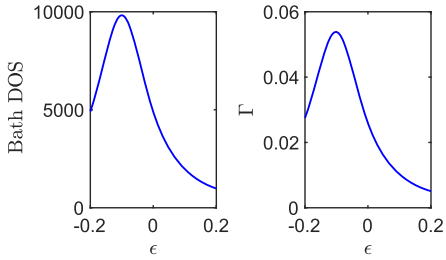

FIG. 5. The density of states (left) and the hybridization function (right) of the quasi-continuous model in Sec. III B. The bath has a total of 2000 states ranging from −0.2 to 0.2. Note that we are now breaking the wideband approximation as Γ depends on ϵ.

Consider a model described by the Hamiltonian in Eq. (5) with the bath density of states and Γ shown in Fig. 5. Figures 6–8 show how Figs. 1, 3, and 4 change with a non-constant DOS and Γ. Given a sufficiently dense bath and a moderate temperature, all methods can recover the exact result (Fig. 6). However, as the bath quasi-continuity deteriorates, broadening methods fail to converge with respect to the broadening parameter. On the contrary, our interpolation is very robust even without a very large number of states and outperforms all broadening methods. It is worth noting that at high temperatures ($k_BT \sim \Gamma$), our method has a small but inherent systematic error that comes from the curve fitting, as can be seen from Fig. 7. As such, broadening methods could perform slightly better than our method if the bath was sufficiently dense. Of course, our error could be lessened by using a more sophisticated functional form than that in Eq. (20) or (24). In general, one should be aware that k_BT (e.g., 0.026 eV at 300 K) is usually much smaller than typical Γ values for most reactions of interest, especially for bond-making and bond-breaking cases. When Γ is nearly

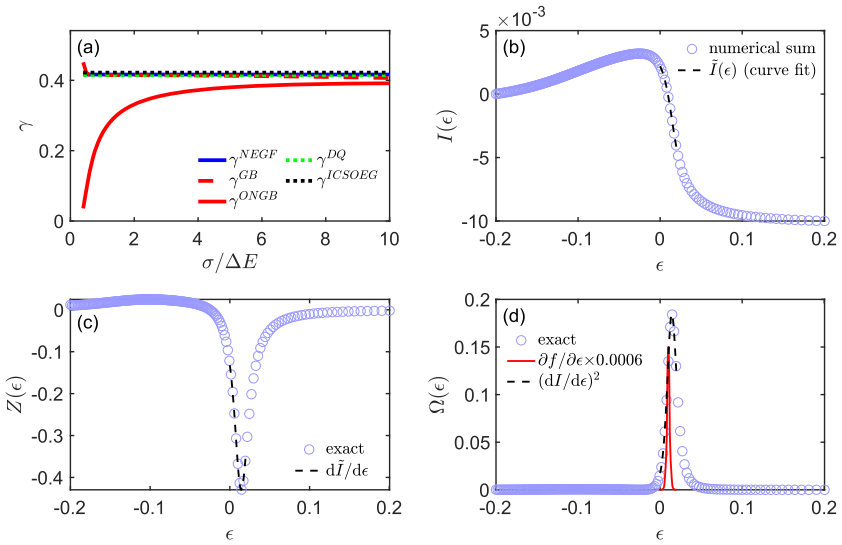

FIG. 6. A quasi-continuous model for the Hamiltonian in Eq. (5). The bath density of states and hybridization function $\Gamma(\epsilon)$ are plotted in Fig. 5. Note that we are now breaking the wideband approximation. Our parameters are as follows: $kT = 0.001$, $h = 0$, $\partial_x h = -0.01$, $\epsilon_F = 0.01$, and $\partial_x\Gamma = -0.2\Gamma$. At the Fermi level, the bath energy spacing $\Delta E_F = 2.24 \times 10^{-4}$, $\Gamma_F = 0.0235$, i.e., $\Gamma_F/\Delta E_F = 105$, $k_BT/\Delta E_F = 4.5$. The quantities plotted in (a)–(d) are the same as those in Fig. 1. Basically all methods agree well with the exact NEGF expression.

Published under license by AIP Publishing

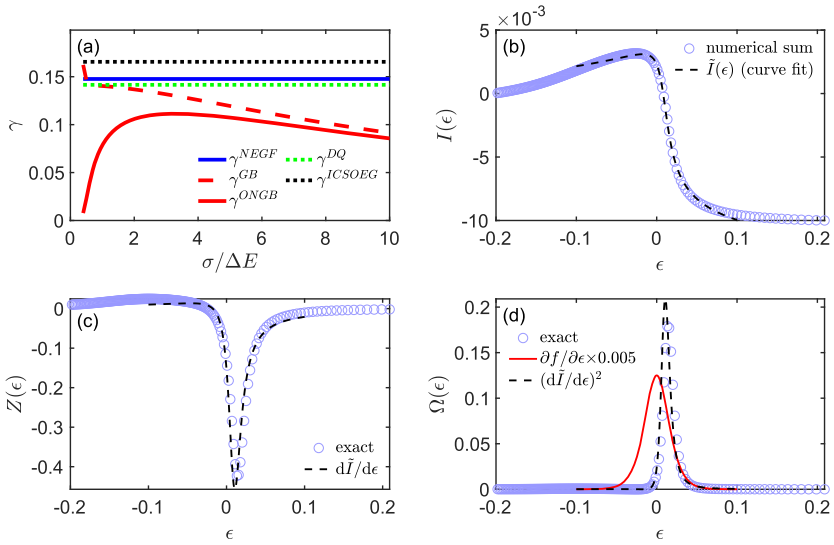

FIG. 7. (a)-(d) Same as in Fig. 6 except that $\epsilon_F = 0$, $kT = 0.01$, and the bath is rescaled to contain only 200 states so that $\Delta E_F = 0.002$ (but note that V_l's are adjusted accordingly so that the overall Γ remains unchanged and still matches that in the right panel of Fig. 5). Here, $\Gamma_F/\Delta E_F = 12.8$, $k_BT/\Delta E_F = 5$. Similar to Fig. 3, the broadening methods fail to converge due to a poor quasi-continuity. Our interpolation method has a 12% error. This error is systematic since the functional form we use is based on a flat-band model and does not globally match an arbitrary quasi-continuous model. The quality of curve fitting, as can be seen from (b)–(d), slightly deteriorates in this high-temperature limit.

equal to k_BT, such an equivalence may well indicate a failure of the adiabatic picture, as does occur, for example, in the case of outer-sphere electron transfer processes. In Fig. 7, a 12% error appears in our interpolation method when $k_BT/\Gamma \sim 0.5$, which we believe to be acceptable for MDEF.

C. Tight-binding model

For our last model, we consider a system containing a molecule and a slab described by a tight binding model with the following Hamiltonian:

$$\begin{aligned}\mathcal{H} &= H_M + H_B + H_{MB} \\ &= h(\boldsymbol{R})d^\dagger d + \sum_{ij} t_{ij}c_i^\dagger c_j + \left(\sum_i V_i(\boldsymbol{R})c_i^\dagger d + \text{h.c.}\right).\end{aligned} \tag{34}$$

Here, d refers to a molecular orbital on the surface, and c_i refers to the localized orbital on slab site i. t_{ij} ($j \neq i$) is the hopping amplitude from slab site j to site i. t_{ii} is the slab on-site energy. V_i is the hopping amplitude between the molecule and slab site i. The large slab should be able to act as its own bath act as its own bath, and we will assume periodic boundary conditions.

In principle, one can generate an arbitrarily dense set of states given enough k points in the Brillouin zone even with a small unit cell. However, as mentioned in Sec. II E 3, this dense set of k points does not necessarily generate a quasi-continuum: because H is block-diagonal in crystal momentum k, the electronic friction tensor is essentially evaluated independently for each k [Eq. (26)] so that the number of bath states used in a curve fit is the number of bands [Eq. (27)]. Thus, the unit cell must be quite large to achieve convergence. As an alternative to Eq. (26), one may use the "k-gathered

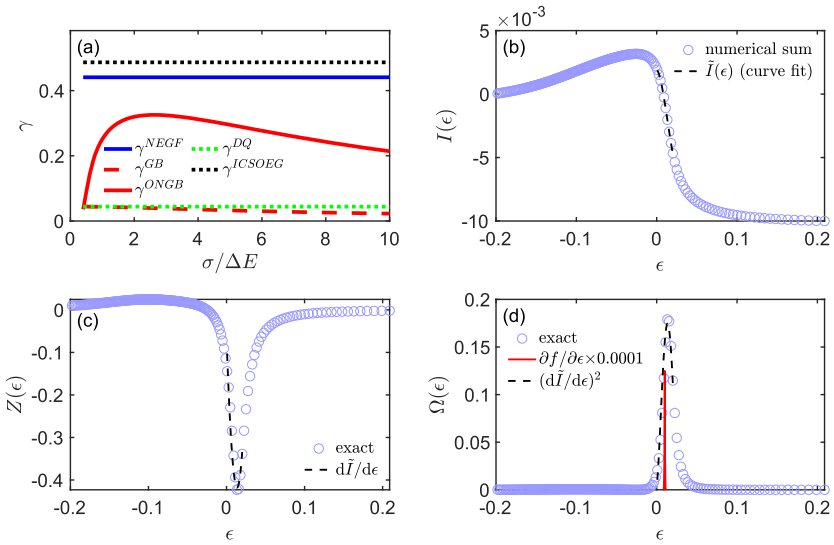

FIG. 8. Same as in Fig. 6 except that $k_BT = 0.0002$ and $\epsilon_F = 0.01$. Here, $\Gamma_F/\Delta E_F = 11.1$, $k_BT/\Delta E_F = 0.09$. This case is similar to that of Fig. 4 insofar as we are undersampling the manifold of electronic states (relatively speaking). As before, our interpolation method is much more robust against this undersampled bath spectrum than are the broadening methods and the direct quadrature.

Published under license by AIP Publishing

approximation" in Sec. II E 3, Eq. (28), which gathers states from all k for a single curve fit at the cost of neglecting the fluctuations of orbital energy gradients within degenerate subspaces.

With that in mind, let us now block-diagonalize Eq. (34). Consider a thin slab of a face-centered cubic lattice containing a few layers along the [111] direction. A block of the Hamiltonian reads

$$\mathcal{H}^{(k)} = h(\boldsymbol{R})d^\dagger d + \sum_{i,j} t_{ij} e^{-i\boldsymbol{k}\cdot\boldsymbol{\delta}} c_i^\dagger c_j + \left(\sum_i V_i(\boldsymbol{R}) c_i^\dagger d + \text{h.c.}\right). \tag{35}$$

Here, $\boldsymbol{k}$ is the crystal momentum, the summation of i and j is taken over the unit cell, and $\boldsymbol{\delta}$ is the lattice vector that connects the home unit cell to the destination unit cell. For intra-cell hoppings $e^{i\boldsymbol{k}\cdot\boldsymbol{\delta}} = 1$, the hopping amplitude is the same as that in Eq. (34); for hoppings that cross the cell boundary, an additional phase ($e^{i\boldsymbol{k}\cdot\boldsymbol{\delta}}$) is multiplied to the original hopping amplitude. To visualize this Hamiltonian, see Fig. 9.

Figures 10 and 11 plot the convergence of the electronic friction tensor with respect to the slab size, the Brillouin zone sampling, and the broadening parameters with different hybridization strength. For each study, γ is computed by the two broadening methods from Sec. II (γ^{GB} and γ^{ONGB}) as well as the interpolation method (γ^{ICSOEG}). γ^{ICSOEG} is plotted for the two different implementations discussed above [k−independent, Eq. (27), and k−gathered, Eq. (28)]. The interpolation method that treats all k states at once (k-gathered) yields very stable results, even for a small unit cell

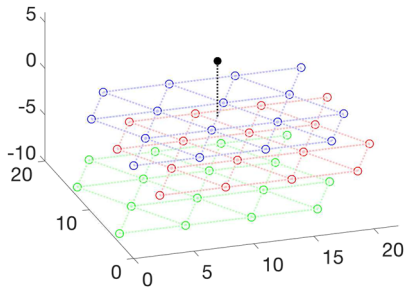

FIG. 9. A schematic diagram of the tight-binding model considered in Sec. III C. The solid black circle is the molecular site. The open circles are the slab sites. The figure contains 3 layers of triangular lattices with 4×4 sites within each layer. Each layer is plotted in a unique color. The molecular site is on top of a bridge position.

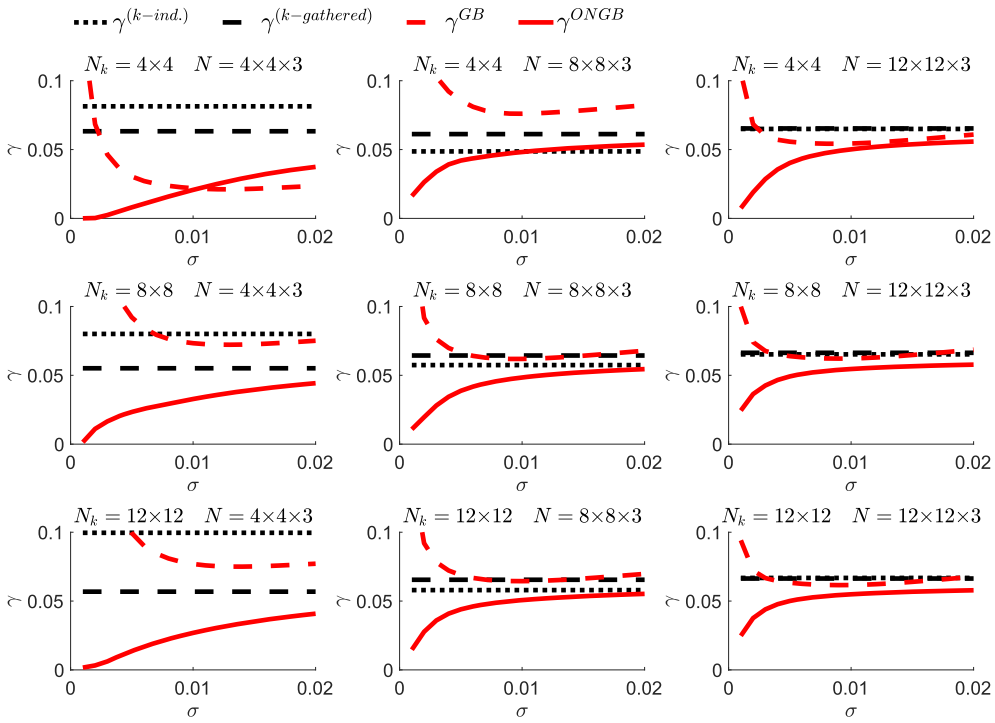

FIG. 10. γ^{GB}(dashed red lines), γ^{ONGB} (solid red lines), γ^{ICSOEG}(k-independent) [Eqs. (25)–(27)] (dotted black lines), and γ^{ICSOEG} (k-gathered) [Eqs. (25) and (28)] (dashed black lines) for the tight-binding model described in Sec. III C. The intra-slab hopping amplitudes between the nearest neighbors are 0.03. The hopping amplitudes between the molecule and the slab sites are assumed to be $V_i = 0.07/(1 + \exp(r_i - 6))$, where r_i is the distance between the molecule and the slab site i. The molecule is placed at a height of 6 above a bridge position of the surface. $kT = 0.001$. The system is assumed to be periodic in the two spatial directions along the surface. The slab sizes and k samplings are labeled above each plot. With a sufficiently large cell and dense Brillouin zone sampling, all methods basically agree. However, with a small cell size and sparse Brillouin zone sampling, the k−gathered interpolation method is the only robust algorithm.

Published under license by AIP Publishing

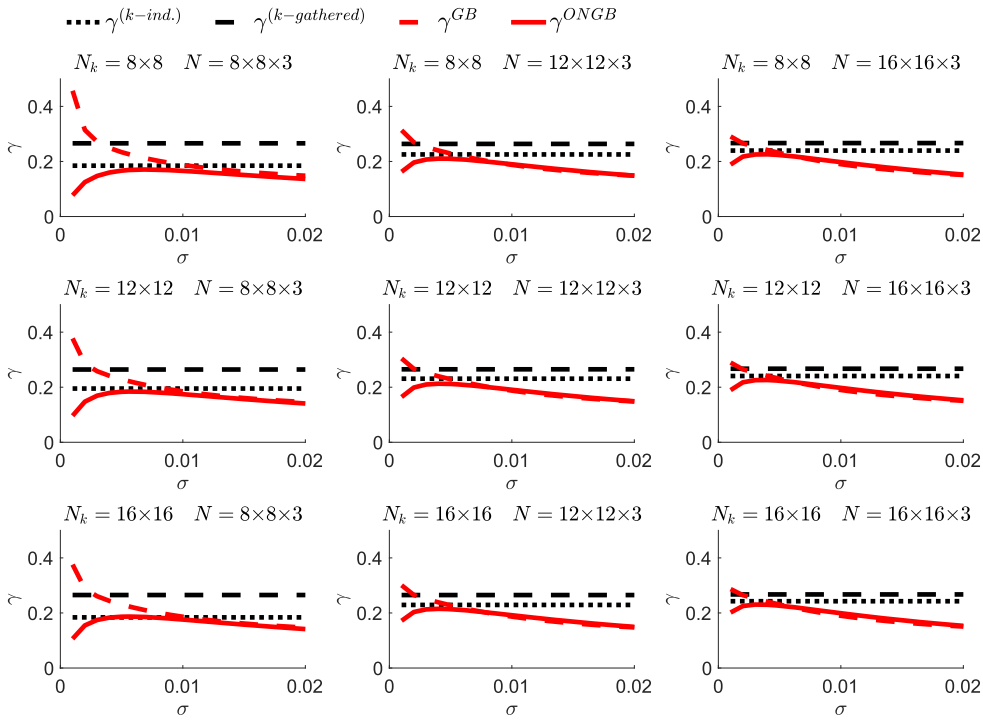

FIG. 11. Same as in Fig. 10 except that $V_i = 0.05/(1 + \exp(r_i - 6))$. With a reduced Γ, the *k*-gathered γ^{ICSOEG} remains relatively stable. This behavior should be contrasted with the case of the two broadening methods, which do not converge with the broadening width even with a slab of 16 × 16 × 6 sites. For this problem, γ^{ICSOEG} with independent *k* approaches γ^{ICSOEG} with gathered *k* at larger cell size.

and few *k* points, as opposed to all of the other methods. In this case, γ^{ICSOEG}'s computed according to the *k*-independent method do tend to approach those computed by the *k*-gathered method for large cell sizes. By contrast, the two broadening methods do not always generate stable results for small cells, though their performance does improve with larger cell size and hybridization Γ. In Fig. 12, we show the details of the curve fitting for the parameter set used in Fig. 11. In particular, we plot the cumulative sum for the *k*−gathered scheme against that for a *k*−independent scheme (at $k = 0$). In the *k*−independent scheme, the number of states that form the supposed quasi-continuum is the number of bands. Without a sufficient number of bands (i.e., a sufficiently large unit cell), the k-independent electronic friction tensors in Figs. 10 and 11 do not fully converge. By contrast, the k-gathered approach converges much faster.

Altogether, these results above strongly encourage the premise that interpolation is a good ansatz for computing electronic friction tensors, and if one is limited by computational cost to reasonably

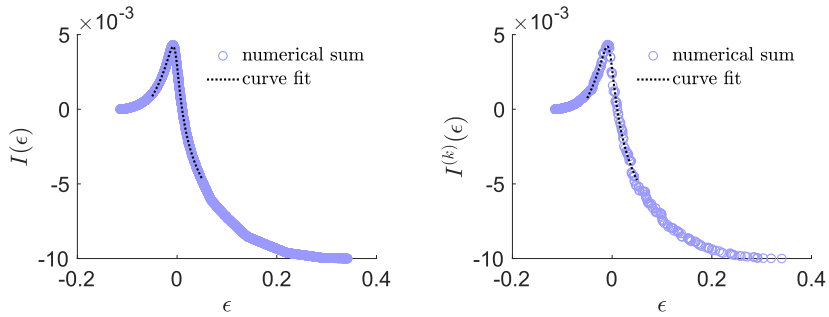

FIG. 12. ICSOEG fit for the tight-binding model with the *k*-gathered (left) and with the *k*-independent (right) scheme (at $k = 0$), $kT = 0.005$. The cell contains 8 × 8 × 6 slab sites and a 10 × 10 Brillouin zone sampling. As can be seen from the right panel, if we separate the electronic states according to crystal momentum k, the resulting data points do not necessarily form a good, smooth quasi-continuum (as is required by a broadening method). Our numerical results suggest that the *k*−gathered scheme can be an optimally efficient and robust approach, provided that the method is a good approximation to the more rigorous k-independent scheme (as is true here).

Published under license by AIP Publishing

small unit cells and few k points, then the most robust approach is the k-gathered formalism.

IV. DISCUSSION

The results above demonstrate that the broadening methods presented in Sec. II are not always robust, particularly when the bath states do not form a good, smooth quasi-continuum. The quality of this quasi-continuum depends on (i) the (average) energy spacing of bath states (ΔE) near the Fermi level, (ii) k_BT, and (iii) the hybridization function Γ. In particular, if either $\Delta E \ll k_BT$ or $\Delta E \ll \Gamma$ is not satisfied, broadening methods can fail to converge with respect to broadening parameters. For *ab initio* methods, we can have no expectation of a good, smooth quasi-continuum when treating a solid made up of realistic electronic bands as opposed to a jellium model. Overall, for the three model studies presented above, broadening methods do not always converge with the broadening parameter, and their relative error can be very large (for example, see Fig. 4). Our tentative conclusion is that broadening methods are not optimal for *ab initio* MDEF.

By contrast, the interpolation method proposed in this study behaves in a relatively robust fashion for all models studied so far. The functional form suggested in Eq. (24), though coming from a wideband analysis, has performed well for a wide range of model parameters. However, based on how the method was hypothesized, there are a few caveats. First, at relatively high temperatures ($k_BT/\Gamma \gtrsim 0.1$), Eq. (24) may not exactly fit the region of interest and introduce a systematic error, as shown in Fig. 7. Second, if the bath spectrum is very narrow, neither Eq. (20) or (24) is guaranteed to provide a good approximation. In both cases, a simple solution would be to use another functional form and check for convergence besides Eqs. (20) and (24).

As for the curve-fitting step, a few points need to be addressed. First, the range of $(\lambda_i, \tilde{I}(\lambda_i))$ used for the curve fitting should be carefully selected. On the one hand, the selected set of $(\lambda_i, \tilde{I}(\lambda_i))$ should be large enough to be identified as a smooth segment of $I(\epsilon)$ and cover the region where $\partial f/\partial\epsilon$ is significant; on the other hand, this set should be as small as possible for efficiency and accuracy (since it is impossible to find a functional form that can match $\tilde{I}(\epsilon)$ for all systems globally). In practice, this set can be selected as follows. First, consider two energy ranges centered around the Fermi level ϵ_F: (i) the range characterized by k_BT and (ii) the range characterized by the average energy spacing (ΔE) near ϵ_F. The actual range that is used to determined the set for curve-fitting should be the larger of the two, e.g., $[\epsilon_F - \max\{5k_BT, 20\Delta E\}, \epsilon_F + \max\{5k_BT, 20\Delta E\}]$. Second, the curve-fitting required by our interpolation method is a nonlinear problem. Although there are quite a few well-established methods that are available, such as the Levenberg-Marquardt algorithm[51–53] or the trust region method,[54,55] we find that a good initial guess is of crucial importance, particularly when the energy range of data points for curve-fitting is much smaller than Γ. In practice, one may first apply a global fitting to obtain a crude parameter set $\{a_i\}$ for Eq. (24) and then use this crude $\{a_i\}$ as the initial guess for a fine curve fitting on the energy range discussed above.

Finally, it should be noted that the above discussions have intrinsically assumed that the electronic friction is a meaningful property of the system at hand and the problem is only computing the EFT. This premise is often the case for gas molecules scattering from a surface, where the bulk solid should provide an ideal bath which cannot be fully captured by *ab initio* calculations with a unit cell of reasonable size. That being said, as stated earlier and well known in the literature, the validity of electronic friction is never guaranteed, especially for the case of small Γ, in which case the requirement of fast electronic equilibration might be violated.[18] Nevertheless, in the future, if we can run MDEF simulations more easily, we will certainly know more about the nature of nonadiabatic surface interactions than we presently know.

Looking forward, we believe the interpolation method presented here can be easily realized in *ab initio* calculations. In practice, according to Eq. (19), all we need are the diagonal matrix elements $\langle j|\partial_\mu \mathcal{H}|j\rangle$, which can be obtained from, for example, density-functional perturbation theory. Such an interpolation method does not rely on any user-identified broadening parameters, which is an enormous advantage for on-the-fly simulations and should make the algorithm compatible with on-the-fly MDEF simulations.

V. CONCLUSION

Even though electronic friction is a universal first order correction to BO theory, with a great deal of development, computing an EFT remains notoriously difficult as the integral expression in Eq. (2) contains two delta functions and demands far more than a DOS calculation. In this study, we have introduced an interpolation method for computing the electronic friction tensors. Benchmark studies against traditional broadening methods suggest that our interpolation method is the most robust option. And unlike traditional methods based on broadening, our interpolation method relies only on orbital energy gradients (rather than derivative couplings) and does not involve any user-identified parameters. These advantages should make this interpolation scheme a good candidate for on-the-fly *ab initio* simulations in a nearly black-box manner.

ACKNOWLEDGMENTS

This work was supported by the U.S. Air Force Office of Scientific Research (USAFOSR) AFOSR Grant No. FA9550-18-1-0497.

REFERENCES

[1] S. P. Rittmeyer, V. J. Bukas, and K. Reuter, "Energy dissipation at metal surfaces," Adv. Phys.: X **3**(1), 1381574 (2018).
[2] H. Nienhaus, H. S. Bergh, B. Gergen, A. Majumdar, W. H. Weinberg, and E. W. McFarland, "Electron-hole pair creation at Ag and Cu surfaces by adsorption of atomic hydrogen and deuterium," Phys. Rev. Lett. **82**, 446–449 (1999).
[3] B. Gergen, N. Hermann, W. Henry Weinberg, and E. W. McFarland, "Chemically induced electronic excitations at metal surfaces," Science **294**(5551), 2521–2523 (2001).
[4] V. N. Ageev, "Desorption induced by electronic transitions," Prog. Surf. Sci. **47**(1), 55–203 (1994).
[5] K. Stépán, J. Güdde, and U. Höfer, "Time-resolved measurement of surface diffusion induced by femtosecond laser pulses," Phys. Rev. Lett. **94**, 236103 (2005).
[6] Y. Huang, C. T. Rettner, D. J. Auerbach, and A. M. Wodtke, "Vibrational promotion of electron transfer," Science **290**(5489), 111–114 (2000).

Published under license by AIP Publishing

[7]B. Oliver, H. Jiang, Y. Dorenkamp, K. Alexander, S. M. Janke, D. J. Auerbach, and A. M. Wodtke, "Electron-hole pair excitation determines the mechanism of hydrogen atom adsorption," Science **350**(6266), 1346–1349 (2015).
[8]B. C. Krüger, N. Bartels, C. Bartels, K. Alexander, J. C. Tully, A. M. Wodtke, and T. Schäfer, "No vibrational energy transfer on a metal surface: Still a challenge to first-principles theory," J. Phys. Chem. C **119**(6), 3268–3272 (2015).
[9]J. R. Trail, D. M. Bird, M. Persson, and S. Holloway, "Electron–hole pair creation by atoms incident on a metal surface," J. Chem. Phys. **119**(8), 4539–4549 (2003).
[10]J. I. Juaristi, M. Alducin, R. Díez Muiño, H. F. Busnengo, and A. Salin, "Role of electron-hole pair excitations in the dissociative adsorption of diatomic molecules on metal surfaces," Phys. Rev. Lett. **100**, 116102 (2008).
[11]S. Neil, S. Roy, and J. C. Tully, "Nonadiabatic dynamics at metal surfaces: Independent-electron surface hopping," J. Chem. Phys. **130**(17), 174107 (2009).
[12]S. P. Rittmeyer, J. Meyer, J. I. Juaristi, and K. Reuter, "Electronic friction-based vibrational lifetimes of molecular adsorbates: Beyond the independent-atom approximation," Phys. Rev. Lett. **115**, 046102 (2015).
[13]M. Askerka, R. J. Maurer, V. S. Batista, and J. C. Tully, "Role of tensorial electronic friction in energy transfer at metal surfaces," Phys. Rev. Lett. **116**, 217601 (2016).
[14]S. P. Rittmeyer, J. Meyer, and K. Reuter, "Nonadiabatic vibrational damping of molecular adsorbates: Insights into electronic friction and the role of electronic coherence," Phys. Rev. Lett. **119**, 176808 (2017).
[15]S. Paul and J. Meyer, "Testing electronic friction models: Vibrational de-excitation in scattering of H_2 and D_2 from Cu(111)," J. Phys. Chem. Lett. **9**(7), 1803–1808 (2018).
[16]A. M. Wodtke, J. C. Tully, and D. J. Auerbach, 'Electronically non-adiabatic interactions of molecules at metal surfaces: Can we trust the born–oppenheimer approximation for surface chemistry?," Int. Rev. Phys. Chem. **23**(4), 513–539 (2004).
[17]M. Head-Gordon and J. C. Tully, "Molecular dynamics with electronic frictions," J. Chem. Phys. **103**(23), 10137–10145 (1995).
[18]W. Dou and J. E. Subotnik, "Perspective: How to understand electronic friction," J. Chem. Phys. **148**(23), 230901 (2018).
[19]E. G. d'Agliano, P. Kumar, W. Schaich, and H. Suhl, "Brownian motion model of the interactions between chemical species and metallic electrons: Bootstrap derivation and parameter evaluation," Phys. Rev. B **11**, 2122–2143 (1975).
[20]B. N. J. Persson and M. Persson, "Vibrational lifetime for co adsorbed on Cu(100)," Solid State Commun. **36**(2), 175–179 (1980).
[21]M. Persson and B. Hellsing, "Electronic damping of adsorbate vibrations on metal surfaces," Phys. Rev. Lett. **49**, 662–665 (1982).
[22]M. Head-Gordon and J. C. Tully, "Vibrational relaxation on metal surfaces: Molecular-orbital theory and application to Co/Cu(100)," J. Chem. Phys. **96**(5), 3939–3949 (1992).
[23]M. Head-Gordon and J. C. Tully, "Molecular-orbital calculations of the lifetimes of the vibrational modes of Co on Cu(100)," Phys. Rev. B **46**, 1853–1856 (1992).
[24]M. Brandbyge, P. Hedegård, T. F. Heinz, J. A. Misewich, and D. M. Newns, "Electronically driven adsorbate excitation mechanism in femtosecond-pulse laser desorption," Phys. Rev. B **52**, 6042–6056 (1995).
[25]J. Daligault and D. Mozyrsky, "Ion dynamics and energy relaxation rate in nonequilibrium electron-ion systems," Phys. Rev. E **75**, 026402 (2007).
[26]B. B. Smith and J. T. Hynes, "Electronic friction and electron transfer rates at metallic electrodes," J. Chem. Phys. **99**(9), 6517–6530 (1993).
[27]N. Bode, S. Viola Kusminskiy, R. Egger, and F. von Oppen, "Scattering theory of current-induced forces in mesoscopic systems," Phys. Rev. Lett. **107**, 036804 (2011).
[28]N. Bode, S. Viola Kusminskiy, R. Egger, and F. von Oppen, "Current-induced forces in mesoscopic systems: A scattering-matrix approach," Beilstein J. Nanotechnol. **3**, 144–162 (2012).
[29]W. Dou, G. Miao, and J. E. Subotnik, "Born-oppenheimer dynamics, electronic friction, and the inclusion of electron-electron interactions," Phys. Rev. Lett. **119**, 046001 (2017).
[30]F. Chen, K. Miwa, and M. Galperin, "Current-induced forces for nonadiabatic molecular dynamics," J. Phys. Chem. A **123**(3), 693–701 (2019).
[31]W. Dou and J. E. Subotnik, "Universality of electronic friction: Equivalence of von oppen's nonequilibrium green's function approach and the head-gordon–tully model at equilibrium," Phys. Rev. B **96**, 104305 (2017).
[32]W. Dou and J. E. Subotnik, "Universality of electronic friction. ii. equivalence of the quantum-classical liouville equation approach with von oppen's nonequilibrium green's function methods out of equilibrium," Phys. Rev. B **97**, 064303 (2018).
[33]F. Giustino, M. L. Cohen, and S. G. Louie, "Electron-phonon interaction using wannier functions," Phys. Rev. B **76**, 165108 (2007).
[34]F. Giustino, "Electron-phonon interactions from first principles," Rev. Mod. Phys. **89**, 015003 (2017).
[35]S. Poncé, E. R. Margine, C. Verdi, and F. Giustino, "Epw: Electron–phonon coupling, transport and superconducting properties using maximally localized wannier functions," Comput. Phys. Commun. **209**, 116–133 (2016).
[36]M. Kawamura, Y. Gohda, and S. Tsuneyuki, "Improved tetrahedron method for the brillouin-zone integration applicable to response functions," Phys. Rev. B **89**, 094515 (2014).
[37]P. E. Blöchl, O. Jepsen, and O. K. Andersen, "Improved tetrahedron method for brillouin-zone integrations," Phys. Rev. B **49**, 16223–16233 (1994).
[38]B. Hellsing and M. Persson, "Electronic damping of atomic and molecular vibrations at metal surfaces," Phys. Scr. **29**(4), 360 (1984).
[39]S. M. Janke, D. J. Auerbach, A. M. Wodtke, and K. Alexander, "An accurate full-dimensional potential energy surface for H–Au(111): Importance of nonadiabatic electronic excitation in energy transfer and adsorption," J. Chem. Phys. **143**(12), 124708 (2015).
[40]D. Novko, M. Blanco-Rey, M. Alducin, and J. I. Juaristi, "Surface electron density models for accurate *ab initio* molecular dynamics with electronic friction," Phys. Rev. B **93**, 245435 (2016).
[41]K. Alexander, H. Jiang, Y. Dorenkamp, S. M. Janke, M. Kammler, A. M. Wodtke, and B. Oliver, "Unified description of H-atom–induced chemicurrents and inelastic scattering," Proc. Natl. Acad. Sci. U. S. A. **115**(4), 680–684 (2018).
[42]R. J. Maurer, M. Askerka, V. S. Batista, and J. C. Tully, "*Ab initio* tensorial electronic friction for molecules on metal surfaces: Nonadiabatic vibrational relaxation," Phys. Rev. B **94**, 115432 (2016).
[43]W. Dou and J. E. Subotnik, "A broadened classical master equation approach for nonadiabatic dynamics at metal surfaces: Beyond the weak molecule-metal coupling limit," J. Chem. Phys. **144**(2), 024116 (2016).
[44]M. Esposito, M. A. Ochoa, and M. Galperin, "Quantum thermodynamics: A nonequilibrium green's function approach," Phys. Rev. Lett. **114**, 080602 (2015).
[45]M. Esposito, M. A. Ochoa, and M. Galperin, "Nature of heat in strongly coupled open quantum systems," Phys. Rev. B **92**, 235440 (2015).
[46]R. W. Godby, M. Schlüter, and L. J. Sham, "Self-energy operators and exchange-correlation potentials in semiconductors," Phys. Rev. B **37**, 10159–10175 (1988).
[47]M. Govoni and G. Galli, "Large scale GW calculations," J. Chem. Theory Comput. **11**(6), 2680–2696 (2015).
[48]M. Galperin and A. Nitzan, "Nuclear dynamics at molecule–metal interfaces: A pseudoparticle perspective," J. Phys. Chem. Lett. **6**(24), 4898–4903 (2015).
[49]I. Loaiza and A. F. Izmaylov, "On the breakdown of the Ehrenfest method for molecular dynamics on surfaces," J. Chem. Phys. **149**(21), 214101 (2018).
[50]Recall that when we move a single atom, we are actually moving the image of the atom in all unit cells. As such, the factor $1/N_k$ arises in Eq. (26) because we seek the friction per unit cell.
[51]K. Levenberg, "A method for the solution of certain non-linear problems in least squares," Q. Appl. Math. **2**(2), 164–168 (1944).
[52]D. W. Marquardt, "An algorithm for least-squares estimation of nonlinear parameters," J. Soc. Ind. Appl. Math. **11**(2), 431–441 (1963).
[53]J. J. Moré, "The Levenberg-Marquardt algorithm: Implementation and theory," in *Numerical Analysis* (Springer, 1978), pp. 105–116.
[54]T. F. Coleman and Y. Li, "On the convergence of interior-reflective Newton methods for nonlinear minimization subject to bounds," Math. Program. **67**(1), 189–224 (1994).
[55]T. Coleman and Y. Li, "An interior trust region approach for nonlinear minimization subject to bounds," SIAM J. Optim. **6**(2), 418–445 (1996).

Published under license by AIP Publishing